

# Computations of radiation force using the translational addition theorem: Applications to acoustical tweezers

André L. Baggio, J. Henrique Lopes, Glauber T. Silva\*

*Physical Acoustics Group, Instituto de Física, Universidade Federal de Alagoas, Maceió,  
AL 57072-900, Brazil*

---

## Abstract

This work proposes a method to compute both axial and transverse radiation forces produced by an ultrasound beam of arbitrary wavefront based on the partial-wave expansion (PWE) and the translational addition theorem for spherical wave functions. The major advantage of using the addition theorem is the computation of acoustic radiation force for a wide variety of beams which satisfy the Helmholtz equation without the need of numerical quadrature schemes. The PWE method is applied to calculate the radiation force exerted on a silicone-oil droplet suspended in water. The force is produced by a single-beam acoustical tweezer composed by a spherically focused transducer with driving frequency of 3.1 MHz and F-number of 1.6. The droplet can be positioned anywhere in the host medium. The radiation force is analyzed in the Rayleigh and resonant scattering regimes. The obtained results in the Rayleigh scattering regime are compared to those calculated with Gor'kov's radiation force theory. It turns out to be that both methods yield similar results for the axial radiation force when ultra-

---

\*Email: glauber@pq.cnpq.br

sound absorption inside the droplet is not considered. However, these results become far apart as the ultrasound absorption is taking into account. In addition, it is shown that the transducer under investigation operates as a single-beam acoustical tweezer in 3D and 2D for the Rayleigh and resonant scattering regimes, respectively.

*Keywords:* Acoustic Radiation Force, Addition Theorem, Acoustical Tweezer

---

## 1. Introduction

The concept of acoustical tweezers is to create a potential well by means of acoustic radiation force where particles can be trapped (Wu, 1991; Lee et al., 2005; Kang and Yeh, 2010). Acoustical tweezers have promising applications in contactless manipulation and trapping of small microorganism such as human cells, bacteria, fungi, protozoa etc. These devices are based on either standing waves (Wu, 1991; Shi et al., 2009; Courtney et al., 2010), or a focused ultrasound beam (Lee et al., 2009).

The underlying physical principle of acoustical tweezers is the radiation force of ultrasound waves. The force exerted by a single-frequency acoustic wave on a suspended object in a nonviscous fluid has been extensively investigated over the last century (Rayleigh, 1902; King, 1934; Embleton, 1954; Yosioka and Kawasima, 1955; Westervelt, 1957; Nyborg, 1967; Hasegawa and Yosioka, 1969; Hasegawa et al., 1988; Chen and Apfel, 1996). The possibility of generating negative axial radiation force by means of limited diffraction Bessel beams have also been studied (Marston, 2006; Mitri, 2009; Azarpeyvand, 2012). In all these studies, the incident beam is assumed to be a running wave that is symmetric with respect to the target object. In other words, the object is supposed to be located in the beam's axis of symmetry. An investigation of the radiation force produced by standing waves of arbitrary wavefront on a small spherical particle (i.e. the Rayleigh scattering regime,  $ka \ll 1$ , where  $k$  is the wavenumber and  $a$  is the sphere's radius) was performed by Gor'kov (1962).

The design of single-beam acoustical tweezers requires an analysis of how radiation force behaves in the vicinity of the device's focus point. So far, this

26 analysis has been only performed in the geometric acoustics regime (Lee and Shung,  
27 2006). A method to compute the radiation force produced by an acoustic  
28 beam with arbitrary wavefront based on the partial-wave expansion (PWE) (Silva,  
29 2011a) can be employed to assist the development of single-beam acousti-  
30 cal tweezers. In the PWE method, radiation force can be obtained in the  
31 Rayleigh  $ka \ll 1$ , resonant  $ka \sim 1$ , and geometric  $ka \gg 1$  scattering regimes.

32 The PWE method for computing radiation force on a suspended sphere  
33 relies on the expansion of the incident and scattered waves in an infinite sum  
34 of wave functions (partial-waves). These expansions are performed in spheri-  
35 cal coordinates with respect to the coordinate system specified, in general,  
36 by the sphere’s center. The complex amplitude of each incident partial-  
37 wave is given in terms of a parameter known as “the beam-shape coefficient”  
38 (BSC) (Gouesbet et al., 1995). The BSCs carry information regarding to  
39 the geometry of the incident beam. Similarly, the scattering coefficients en-  
40 dow the scattered PWE with the mechanical properties of the scatter. The  
41 scattering coefficients can be determined in terms of the BSCs by applying  
42 appropriate boundary conditions across the fluid-object interface. After cal-  
43 culating the beam-shape and scattering coefficients, one can compute the  
44 acoustic radiation force exerted on an object by using the radiation force  
45 formula derived by Silva (2011a). By that means, the BSCs need to be ob-  
46 tained for a specific incident beam in order to enable the computation of the  
47 corresponding radiation force.

48 A single-beam acoustical tweezer employs a focused transducer to gen-  
49 erate an ultrasound beam which may trap suspended particles in the focal  
50 region. The radiation force exerted by the focused beam on a particle located

51 anywhere in the host medium can be obtained by calculating the BSCs with  
52 respect to the particle's position. Computations of the BSCs have been done  
53 through the midpoint integral rule (Silva, 2011b; Mitri and Silva, 2011) and  
54 the discrete spherical harmonics transform (Silva et al., 2012a,b). Numerical  
55 computations of the BSCs requires that the amplitude of the incident pres-  
56 sure be sampled over a virtual a sphere which encloses the beam propagation  
57 region (interior problem). In turn, spatial sampling may induce numerical  
58 error such as aliasing. In order to circumvent numerical approximations and  
59 error, this work proposes a method to compute acoustic radiation force based  
60 on the PWE and the translational addition theorem (Martin, 2006, ch. 3).  
61 The method is used to calculate the radiation force produced by a spherically  
62 focused transducer on a silicone-oil droplet. The transducer has F-number  
63 of 1.6 and operates at 3.1 MHz. Using closed-form expressions of the BSCs  
64 with respect to the transducer focus point (Edwards and Jarzynski, 1983),  
65 both axial and transverse radiation forces are computed in the vicinity of  
66 transducer'ss depth-of-field. The Rayleigh and resonant scattering regimes  
67 are considered in this analysis. The results obtained for the Rayleigh scat-  
68 tering regime are compared to those computed from Gor'kov's theory. A  
69 significant deviation from Gor'kov's theory is found in the axial radiation  
70 force when ultrasound absorption in the droplet is taken into account. In  
71 addition, transverse trapping is achieved in both Rayleigh and resonant scat-  
72 tering regimes. Although, simultaneous axial and transverse trapping only  
73 happens for droplets in the Rayleigh scattering regime.

74 **2. Physical model**

75 Consider an acoustic beam of arbitrary wavefront with angular frequency  
 76  $\omega$  that propagates in a nonviscous infinite fluid. The fluid has ambient density  
 77  $\rho_0$  and speed of sound  $c_0$ . The acoustic beam is described by the excess of  
 78 pressure  $p$  as a function of position vector  $\mathbf{r}$ , with respect to some coordinate  
 79 system, and time  $t$ . An spherical scatterer with radius  $a$ , density  $\rho_1$ , and  
 80 speed of sound  $c_1$  is placed in the beam path. For the sake of simplicity,  
 81 acoustic streaming in the vicinity of the sphere are assumed to be negligible.

82 *2.1. Scattering problem*

83 An spherically focused transducer with diameter  $2b$  and curvature radius  
 84  $z_0$  is used to produce a focused beam to the sphere (see Fig. 1). The origin  
 85 of the coordinate system  $O$  is set in the sphere's center. The scattering of  
 86 the incident beam by the sphere located in the transducer focus is referred  
 87 to as the on-focus scattering configuration (Edwards and Jarzynski, 1983).

88 In the on-focus scattering formalism, the normalized amplitude of the  
 89 incident pressure beam can be described in spherical coordinates  $(r, \theta, \varphi)$  by  
 90 the following PWE (Williams, 1999, Eq. 6.140)

$$\hat{p}_i = \sum_{n,m} a_n^m j_n(kr) Y_n^m(\theta, \varphi), \quad (1)$$

91 where  $\sum_{n,m} = \sum_{n=0}^{\infty} \sum_{n=-m}^m$ ,  $a_n^m$  is the BSC to be determined,  $k = \omega/c_0$ ,  $j_n$   
 92 is the  $n$ th-order spherical Bessel function, and  $Y_n^m$  is the spherical harmonic  
 93 of  $n$ th-order and  $m$ th-degree. Note that the amplitude is normalized to the  
 94 pressure magnitude  $p_0$ . Using the orthonormality properties of the spherical

95 harmonics, the BSCs are obtained from Eq. (1) as

$$a_n^m = \frac{1}{j_n(kR)} \int_{\Omega} \hat{p}_i(kR, \theta, \varphi) Y_n^{m*}(\theta, \varphi) d\Omega, \quad (2)$$

96 where  $R$  is the radius of a virtual spherical region where the beam propagates,  
97  $d\Omega$  is the differential solid angle, and  $\Omega = \{(\theta, \varphi) : 0 \leq \theta \leq \pi, 0 \leq \varphi \leq 2\pi\}$ .

98 The integral in Eq. (2) can be evaluated by numerical quadrature.

99 Suppose now that the sphere is translated to a new point denoted by a  
100 vector  $\mathbf{d}$  as shown in Fig. 1. This corresponds to the off-focus scattering by  
101 the sphere. In spherical coordinates, the translational vector  $\mathbf{d}$  is represented  
102 with respect to the system  $O'$  by  $(d, \theta_d, \varphi_d)$ . Now, the sphere's center defines  
103 a new coordinate system denoted by  $O$ . The incident beam can be described  
104 in a new spherical coordinate system  $(r', \theta', \varphi')$  as

$$\hat{p}_i = \sum_{\nu, \mu} a_{\nu}^{\mu'} j_{\nu}(kr') Y_{\nu}^{\mu}(\theta', \varphi'), \quad (3)$$

105 where  $a_{\nu}^{\mu'}$  is called the translational BSC. A similar expression to Eq. (2) can  
106 be obtained for the translational BSC by using the orthogonality property of  
107 spherical harmonics.

108 The relation between the position vectors of the  $O$  and  $O'$  coordinate  
109 systems is  $\mathbf{r} = \mathbf{r}' + \mathbf{d}$ . The translational addition theorem between the wave  
110 functions in the systems  $O$  and  $O'$  states that (Martin, 2006, Eq. 3.78)

$$j_n(kr) Y_n^m(\theta, \varphi) = \sum_{\nu, \mu} S_{n\nu}^{m\mu}(k\mathbf{d}) j_{\nu}(kr') Y_{\nu}^{\mu}(\theta', \varphi'), \quad (4)$$

where the separation matrix is given by

$$\begin{aligned} S_{\nu n}^{\mu m}(k\mathbf{d}) &= 4\pi (-1)^m \sum_{q=|n-\nu|}^{n+\nu} i^{q+n-\nu} \mathcal{G}(\nu, \mu; n, -m; q) \\ &\times j_q(kd) Y_q^{\mu-m}(\theta_d, \varphi_d), \end{aligned} \quad (5)$$

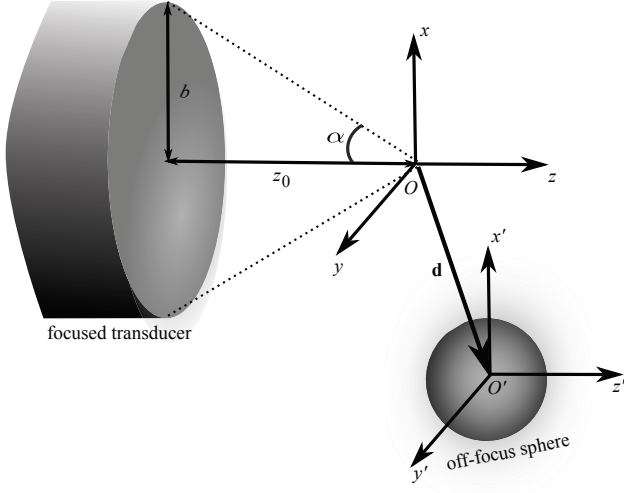


Figure 1: Sketch of the acoustic scattering by a sphere placed anywhere in the host medium. The systems  $O$  and  $O'$  correspond to the on- and off-focus scattering configurations.

111 with  $\mathcal{G}$  being the Gaunt coefficient (Martin, 2006, Eq. 3.73). This coefficient  
 112 is zero if any of the following conditions happens  $n + \nu + q$  is odd,  $q > \nu + n$ ,  
 113 or  $q < |n - \nu|$ .

114 Now, substituting Eq. (4) into Eq. (1) and use the result in Eq. (2) one  
 115 obtains the translational BSCs as

$$a_{\nu}^{\mu'} = \sum_{n,m} a_n^m S_{\nu n}^{\mu m}(k\mathbf{d}), \quad (6)$$

116 where  $\nu = 0, 1, \dots, \infty$  and  $-\nu \leq \mu \leq \nu$ . Note that each translational BSC is  
 117 a combination of all possible BSC with respect to the system  $O$ .

118 Now, the scattered pressure is considered. Assume that the sphere is  
 119 located in the transducer's focus point (on-focus scattering configuration).  
 120 The amplitude of the scattered pressure is described by the following expan-

121 sion (Williams, 1999, Eq. 6.92)

$$\hat{p}_s = \sum_{n,m} s_n^m h_n^{(1)}(kr) Y_n^m(\theta, \varphi), \quad (7)$$

122 where  $s_n^m$  is the scattering coefficient,  $h_n^{(1)}$  is the  $n$ th-order spherical Hankel  
 123 function of first type. Considering a compressional sphere, the scattering  
 124 coefficient is determined from the continuity condition for the pressure and  
 125 the particle velocity across the sphere's surface. Further details can be seen  
 126 in (Anderson, 1950). Thus, using the aforementioned boundary conditions  
 127 one obtains

$$s_n^m = a_n^m s_n, \quad (8)$$

where

$$s_n = -\det \begin{bmatrix} \gamma j_n(ka) & j_n(k_1a) \\ j_n'(ka) & j_n'(k_1a) \end{bmatrix} \times \det \begin{bmatrix} \gamma h_n^{(1)}(ka) & j_n(k_1a) \\ h_n^{(1)'}(ka) & j_n'(k_1a) \end{bmatrix}^{-1}, \quad (9)$$

128 with  $\gamma = \rho_0 k_1 / (\rho_1 k)$ . The prime symbol indicates differentiation. According  
 129 to Eq. (8) the scattering coefficient depends on the BSC with respect to the  
 130 system  $O$  and on a function ( $s_n$ ) of the sphere mechanical parameters. This  
 131 function is independent of the choice of the coordinate system. Therefore, in  
 132 the system  $O'$  the scattering coefficient becomes

$$s_n^{m'} = a_n^{m'} s_n. \quad (10)$$

133 Ultrasound absorption effects inside the sphere is considered by including  
 134 an imaginary part in the wavenumber as follows

$$k_1 = \frac{\omega}{c_1} + i\alpha_0, \quad (11)$$

135 where  $\alpha_0$  is the absorption coefficient. It is worthy to notice that shear wave  
 136 propagation inside the sphere is neglected.

137 *2.2. Focused transducer in the paraxial approximation*

138 In adopting the paraxial approximation for the spherically focused trans-  
 139 ducer, it is assumed that  $b^2 \ll z_0^2$ . Futhermore, the transducer is excited  
 140 with a uniform velocity distribution  $v_0$ . In terms of the Rayleigh integral,  
 141 the amplitude of the pressure generated by the transducer is given by (Pierce,  
 142 1989, p. 215)

$$\hat{p}_i = -\frac{ik\rho_0 c_0 v_0}{2\pi} \int_S \frac{e^{ik|\mathbf{r}-\mathbf{r}'|}}{|\mathbf{r}-\mathbf{r}'|} dS', \quad (12)$$

143 where  $S$  is the surface of the transducer's active element. Hereafter, the  
 144 pressure amplitude is normalized to  $p_0 = \rho_0 c_0 v_0$ .

145 To derive the on-focus BSC, the origin of the coordinate system is sup-  
 146 posed to be in the transducer focal point. By assuming that  $r < z_0$ ,  $kz_0 \gg 1$ ,  
 147 and  $\|\mathbf{r}'\| = z_0$ , the following expansion is used (Colton and Kress, 1998,  
 148 Eq. 2.42)

$$\begin{aligned} \frac{e^{ik|\mathbf{r}-\mathbf{r}'|}}{|\mathbf{r}-\mathbf{r}'|} &= 4\pi \frac{e^{ikz_0}}{z_0} \sum_{n,m} (-i)^n j_n(kr) \\ &\times Y_n^m(\theta', \varphi') Y_n^{m*}(\theta, \varphi) \end{aligned} \quad (13)$$

into Eq. (12). Thus, integrating in the angular variables  $(\theta', \varphi')$  yields

$$\begin{aligned} \hat{p}_i &= -ikz_0 e^{ikz_0} \sum_{n=0}^{\infty} i^n \sqrt{\frac{4\pi}{2n+1}} \\ &\times [P_{n+1}(\cos \alpha) - P_{n-1}(\cos \alpha)] j_n(kr) Y_n^0(\theta, \varphi), \end{aligned} \quad (14)$$

149 where  $\alpha = \arcsin(b/r_0)$  is the half-spread angle of the transducer and  $P_n$   
 150 is Legendre polynomial function of order  $n$ . The on-focus BSC is found by

151 comparing Eqs. (1) and (14). Accordingly,

$$\begin{aligned}
 a_l^m &= -i^{(n+1)} k r_0 e^{i k r_0} \sqrt{\frac{4\pi}{2n+1}} \\
 &\times [P_{n+1}(\cos \alpha) - P_{n-1}(\cos \alpha)] \delta_{m,0}.
 \end{aligned}
 \tag{15}$$

152 The PWE of the focused beam can be compared to some analytical re-  
 153 sults. Let the radial distance in cylindrical coordinates be given by  $\varrho =$   
 154  $\sqrt{x^2 + y^2}$ . The pressure produced by the transducer in the focal plane is  
 155 given by (Lucas and Muir, 1982)

$$p_i(\varrho, 0) = i \left( \frac{b}{\varrho} \right) \exp \left[ i k \left( \frac{\varrho^2}{z_0} + z_0 \right) \right] J_1(k\varrho \sin \alpha),
 \tag{16}$$

156 where  $J_1$  is the first-order Bessel function. Along the transducer's axis, we  
 157 have

$$p_i(0, z) = \frac{i z_0}{z - z_0} \left\{ 1 - \exp \left[ \frac{i k b^2}{2} \left( \frac{1}{z} - \frac{1}{z_0} \right) \right] \right\}.
 \tag{17}$$

### 158 3. Acoustic radiation force

159 After calculating both the incident and scattered acoustic fields through  
 160 the PWE method, the radiation force can be calculated by integrating the  
 161 radiation stress tensor  $\mathbf{S}$  over the scatter's surface. In second-order approxi-  
 162 mation, the radiation stress tensor is given by

$$\mathbf{S} = \rho_0 \overline{\mathbf{v}\mathbf{v}} - \left( \frac{\rho_0 \overline{v^2}}{2} - \frac{\overline{p^2}}{2\rho_0 c_0^2} \right) \mathbf{I},
 \tag{18}$$

163 where the overbar denotes time-average,  $\rho_0 \mathbf{v}\mathbf{v}$  is the Reynolds' stress tensor,  
 164  $v = \|\mathbf{v}\|$ , and  $\mathbf{I}$  is the  $3 \times 3$ -unit matrix. Considering a nonviscous fluid, the  
 165 radiation stress tensor is a zero divergent quantity, i.e.  $\nabla \cdot \mathbf{S} = 0$ . Thus, by  
 166 using the Gauss divergence theorem one can show that the radiation force is

167 given by integrating the radiation stress tensor on a control spherical surface  
 168 centered at the target object. Furthermore, the radius of the control surface  
 169  $r$  lies in the farfield, i.e.  $kr \gg 1$ . Therefore, the radiation force is given by

$$\mathbf{f} = -r^2 \int_{\Omega} \mathbf{S} \cdot \mathbf{e}_r d\Omega, \quad kr \gg 1, \quad (19)$$

170 where  $\mathbf{e}_r$  is the radial unit-vector, and  $d\Omega$  is the differential solid angle.  
 171 One can show that the Cartesian components of the radiation force can be  
 172 expressed as (Silva, 2011a)

$$\mathbf{f} = \pi a^2 E_0 (Y_x \mathbf{e}_x + Y_y \mathbf{e}_y + Y_z \mathbf{e}_z), \quad (20)$$

173 where  $E_0 = p_0^2 / (2\rho_0 c_0^2)$  is the characteristic energy density of the incident  
 174 wave. The radiation force functions are given by

$$\begin{aligned} Y_x + iY_y &= \frac{i}{2\pi(ka)^2} [(a_l^{m*} + s_l^{m*})(s_{l+1}^{m-1} b_{l+1}^{-m} \\ &+ s_{l-1}^{m-1} b_l^{m-1}) + (a_l^m + s_l^m) \\ &\times (s_{l+1}^{m+1} b_{l+1}^m + s_{l-1}^{m+1} b_l^{-m-1})], \quad (21) \\ Y_z &= \frac{1}{\pi(ka)^2} \text{Im} \sum_{l,m} (a_l^m + s_l^m) \\ &\times (s_{l+1}^{m*} c_{l+1}^m - s_{l-1}^{m*} c_l^m), \end{aligned}$$

175 where ‘Im’ denotes the imaginary part of a complex number, and the symbol  
 176 \* means complex conjugation. Furthermore,

$$b_l^m = \sqrt{\frac{(l+m)(l+m+1)}{(2l-1)(2l+1)}}, \quad (22)$$

$$c_l^m = \sqrt{\frac{(l-m)(l+m)}{(2l-1)(2l+1)}}. \quad (23)$$

177 **4. Results and discussion**

178 Consider that the ultrasound beam is generated in water for which  $c_0 =$   
 179  $1500 \text{ m/s}$  and  $\rho_0 = 1000 \text{ kg/m}^3$ . The focused transducer has radius  $b =$   
 180  $22 \text{ mm}$ , F-number of 1.6, and operates at  $3.1 \text{ MHz}$ . The magnitude of the  
 181 pressure generated by the transducer is  $p_0 = \rho_0 c_0 v_0 = 10^5 \text{ Pa}$ . A droplet  
 182 made out of silicone-oil ( $c_1 = 974 \text{ m/s}$ ,  $\rho_1 = 1004 \text{ kg/m}^3$ , and  $\alpha_0 = 21 \text{ Np/m}$   
 183 at  $3.1 \text{ MHz}$ ) is used as the target object.

184 The truncation error in computing the translational BSCs in Eq. (6) is  
 185 analyzed in Appendix A. Accordingly, the truncation order for the index  $n$   
 186 necessary to achieve a certain error  $\epsilon$  is given by

$$N = \nu + kd + 1.8(\log \epsilon^{-1})^{2/3}(kd)^{1/3}. \quad (24)$$

187 The error considered in the translational BSC computations is  $\epsilon = 10^{-6}$ . The  
 188 truncation order  $L$  of the radiation force series in (21) is established by the  
 189 scattering coefficient ratio  $|s_L^m/s_0^0| < 10^{-7}$ . This condition ensures proper  
 190 convergence of the radiation force series.

191 In Fig. 2, the pressure amplitude (normalized to  $p_0$ ) produced by the fo-  
 192 cused transducer is shown along  $x$  and  $z$  directions. The pressure is computed  
 193 using the PWE and analytical method based on Eq. (16). Good agreement  
 194 is found between the methods in the transverse direction and in the vicinity  
 195 of the focal region. Though moving away from the focal region, the PWE  
 196 method starts to deviate from the analytical result.

197 Figure 3 exhibits the axial radiation force versus the droplet's position  
 198 along the transducer's axis ( $z$  direction). The droplet's size factors are  
 199  $ka = 0.1$  (Rayleigh regime) and  $ka = 0.5$  (resonant regime). The solid

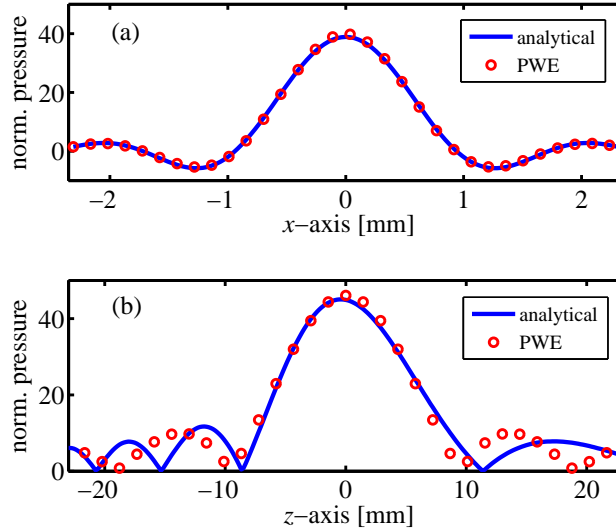


Figure 2: Pressure amplitude generated by the spherically focused transducer with aperture 44 mm and F-number of 1.6, operating at 3.1 MHz. The pressure is evaluated along (a) the transverse and (b) the axial directions.

200 line represents the radiation force computed with Gor'kov's method. Good  
 201 agreement between the methods is found when no ultrasound absorption  
 202 is considered in the droplet. However, when ultrasound absorption is tak-  
 203 ing into account, a significant deviation between these methods is observed.  
 204 This result is expect since the acoustic radiation force caused by a plane  
 205 running wave on a sphere depends on the sum of the scattered and absorbed  
 206 power (Westervelt, 1957). Therefore, if absorption is taking into account the  
 207 radiation force will be larger than in the case where absorption is neglected.  
 208 The droplet with with  $ka = 0.1$  might be axially trapped along the trans-  
 209 ducer axis at  $z = 2.5$  mm (with absorption). Note that a nonviscous droplet  
 210 would be trapped at  $z = 0$ . Gor'kov's method no longer describes the behav-

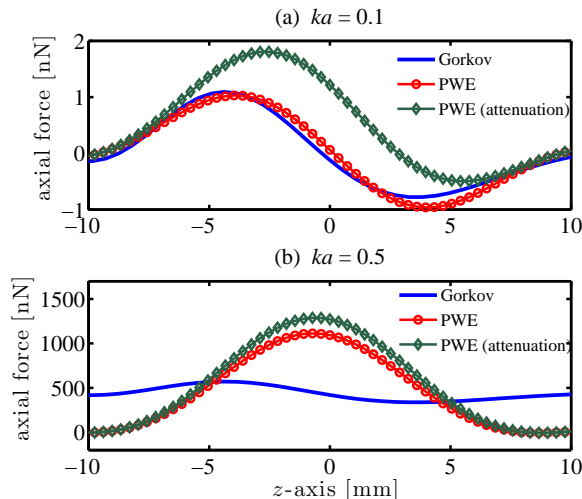


Figure 3: Axial radiation force versus the droplet’s position along  $z$  direction in the focal plane. The force is computed through the PWE and Gor’kov’s methods. The size factors of the sphere are (a)  $ka = 0.1$  and (b)  $ka = 0.5$ .

211 ior of the radiation force generated by the focused transducer when  $ka = 0.5$ .  
 212 Furthermore, it is not possible to axially trap the droplet with the analyzed  
 213 transducer at this size factor. This can be understood as follows. The radia-  
 214 tion force on a small particle is formed by two contributions (Gor’kov, 1962):  
 215 “the scattering force” caused mostly by the running wave in the beam and  
 216 “the gradient force” due to the stationary pattern of the beam. As the size  
 217 factor increases, so does the scattering force. When this force overcomes  
 218 the gradient force, the axial trapping is no longer possible. This might be  
 219 prevented using tightly focused beams (Lee et al., 2009).

220 The transverse radiation force versus the droplet’s position along  $x$  di-  
 221 rection in the focal plane is shown in Fig. 4. Excellent agreement is found  
 222 between the PWE and Gor’kov’s methods when  $ka = 0.1$ . Some deviation

223 between the methods arises when  $ka = 0.5$ . Note that the results with and  
 224 without attenuation are very close. The transverse trapping happens for  
 225 both  $ka = 0.1$  and  $0.5$ , because no scattering radiation force is present in the  
 226 transverse direction. Only the gradient radiation force appears in this direc-  
 227 tion. Based on Figs. 3 and 4, we conclude that the focused transducer forms  
 228 a 3D acoustical tweezer for silicone-oil droplets in the Rayleigh scattering  
 regime.

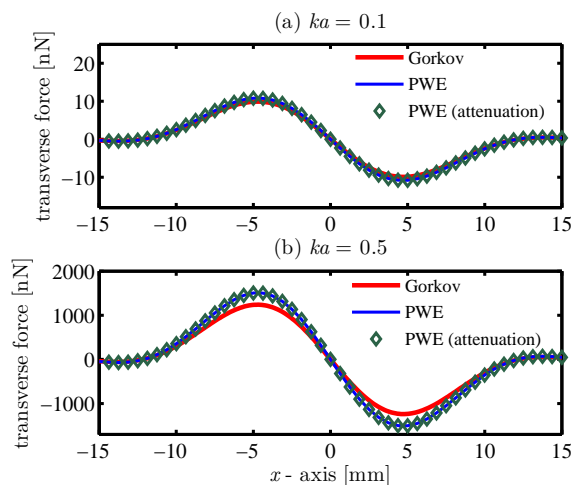


Figure 4: Transverse radiation force versus the droplet’s position along  $x$  direction in the focal plane. The force is computed through the PWE and Gor’kov’s methods. The size factors are (a)  $ka = 0.1$  and (b)  $ka = 0.5$ .

229

230 The axial radiation force versus the droplet’s position along  $z$  direction for  
 231 the resonant scattering regime ( $ka = 1, 5$ ) is shown in Fig. 5. For the case in  
 232 study, the scattering force totally overcomes the gradient force. Thereby, no  
 233 trapping is possible in the axial direction with the analyzed transducer. The  
 234 axial radiation force pushes the droplet to the forward scattering direction.

235 In Fig. 6, the transverse radiation force versus the droplet’s position along

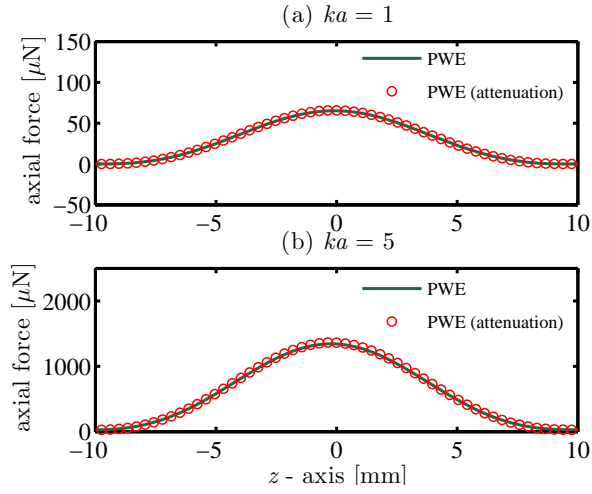


Figure 5: Axial radiation force versus the droplet's position along  $z$  direction for the resonant scattering regime (a)  $ka = 1$  and (b)  $ka = 5$ .

236  $x$  direction is exhibited for the resonant scattering regime ( $ka = 1$  and 5).  
 237 It is clearly shown that transverse trapping is still possible in this regime.  
 238 This happens because the incident beam is tightly focused in the transverse  
 239 direction. Moreover, the transverse radiation force remains practically the  
 240 same considering regardless ultrasound attenuation in the droplet.

241 The vector field of the transverse radiation force on the silicone-oil droplet  
 242 placed in the transducer focal plane is displayed in Fig. 7. The background  
 243 map represents the axial radiation force exerted on the droplet. If the droplet  
 244 lies in the circular region with radius of 0.5 mm around the focus point, it  
 245 will be attracted and trapped in the transducer's axis. The droplet will be  
 246 further pushed by a force of about  $60 \mu\text{N}$ . Therefore, the focused transducer  
 247 operates as a 2D acoustical tweezer for droplets in the resonant scattering  
 248 regime ( $ka = 1$ ).

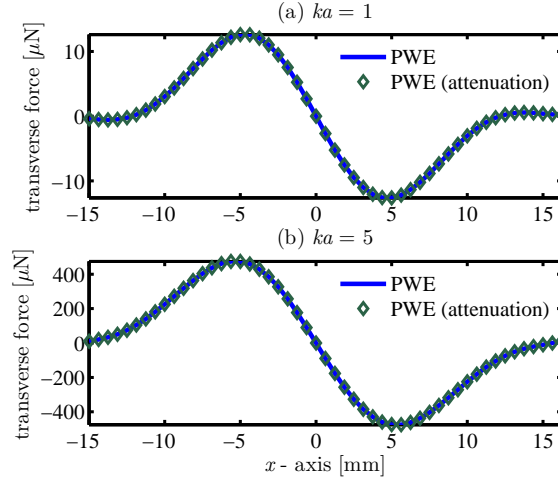


Figure 6: Transverse radiation force on a silicone oil droplet (with and without attenuation) in the resonant scattering regime (a)  $ka = 1$  and (b)  $ka = 5$ .

## 249 5. Summary and conclusion

250 A method to compute acoustic radiation force based on the PWE and the  
 251 translational addition theorem for spherical wave functions was presented.  
 252 The method relies on the fact that once the BSCs are known with respect  
 253 to a coordinate system, they can be calculate for a new coordinate system  
 254 defined by a translation of the former system. The radiation force generated  
 255 by an ultrasound focused beam in the paraxial approximation and exerted  
 256 on a silicone-oil droplet placed anywhere in the host medium was calculated  
 257 using the proposed method. Both axial and transverse radiation forces were  
 258 computed in the Rayleigh and resonant scattering regimes. In the Rayleigh  
 259 regime, the obtained results were compared to Gor'kov's method to calcu-  
 260 late radiation force. Good agreement was found between the methods when  
 261 ultrasound absorption inside the droplet was neglected. Nevertheless, a sig-

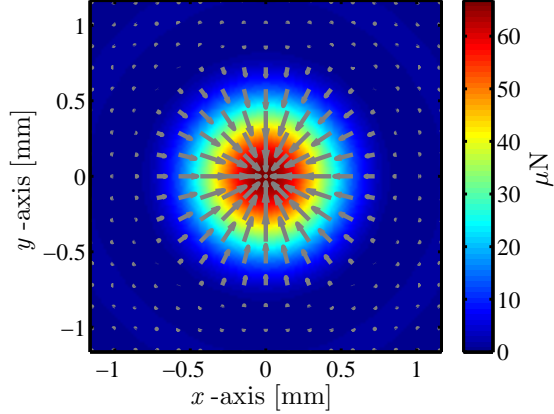


Figure 7: Transverse radiation force vector field in the transducer focal plane produced on the silicone oil droplet in the resonant regime  $ka = 1$ . The vector field is plot on top of the axial radiation force.

262 nificant deviation between the results takes place in the axial radiation force  
 263 when the ultrasound absorption is considered. The transducer under inves-  
 264 tigation, with driving frequency of 3.1 MHz and F-number of 1.6, operated  
 265 as a single-beam acoustical tweezer in 3D for the Rayleigh scattering regime.  
 266 In contrast, only transverse trapping of the silicone-oil droplet was achieved  
 267 for the resonant scattering regime.

268 In conclusion, the translational addition theorem of spherical wave func-  
 269 tions was used with the PWE to compute acoustic radiation force. This  
 270 method may become a helpful tool in assisting the design and evaluation of  
 271 acoustical tweezers.

272 **Acknowledgements**

273 This work was supported by grants CAPES 2163/2009-AUX-PE-PNPD,  
 274 CNPq 306697/2010-6, CNPq 477653/2010-3 (Brazilian agencies). We would  
 275 like to thank Dr. F. G. Mitri for helpful discussions.

276 **Appendix A. Truncation error**

277 Assume the series in Eq. (6) is truncated in  $n = N$ . Thus, the truncation  
 278 error is given by

$$\epsilon = \left| \sum_{n=N+1}^{\infty} \sum_{m=-n}^n a_n^m S_{\nu n}^{\mu m}(k\mathbf{d}) \right|. \quad (\text{A.1})$$

279 We consider the truncation error for a plane progressive wave. This anal-  
 280 ysis as the upper limit case for the error because the normalized pressure  
 281 amplitude of an acoustic beam is smaller than that of a normalized plane  
 282 wave. The beam-shape coefficient of a plane wave described by  $\hat{p} = e^{ikz}$  is  
 283  $a_n^m = i^n \sqrt{4\pi(2n+1)}\delta_{m,0}$ . Substituting this into Eq. (A.1) yields

$$\epsilon = \sqrt{4\pi} \left| \sum_{n=N+1}^{\infty} i^n \sqrt{2n+1} S_{\nu n}^{\mu,0}(k\mathbf{d}) \right|. \quad (\text{A.2})$$

The leading term of the separation matrix in Eq. (5) is related to the spherical Bessel function of smallest order, i.e.  $q = |n - \nu|$ . Therefore, the truncation error can be approximated to

$$\begin{aligned} \epsilon \simeq (4\pi)^{3/2} \sqrt{2N - 2\nu + 3} & \left| \mathcal{G}(\nu, \mu; N + 1, 0; N - \nu + 1) \right. \\ & \left. \times j_{N-\nu+1}(kd) Y_{N-\nu+1}^{\mu}(\theta_d, \varphi_d) \right|. \end{aligned} \quad (\text{A.3})$$

284 After integrating over  $(\theta_d, \varphi_d)$ , we obtain

$$\epsilon \simeq |j_{N-\nu+1}(kd)|. \quad (\text{A.4})$$

When the order of the spherical Bessel function is larger than its argument, the error can be approximated to (Song and Chew, 2001)

$$\epsilon \simeq \left| \frac{1}{2} \sqrt{\frac{1}{xf(x, L)}} \exp \left[ f(x, L) - \left( L + \frac{3}{2} \right) \ln \left( L + \frac{3}{2} + \frac{f(x, L)}{x} \right) \right] \right|, \quad (\text{A.5})$$

285 where  $L = N - \nu + 1$ ,  $x = kd$ , and  $f(x, L) = \sqrt{(L + 3/2)^2 - x^2}$ . We define  
 286  $L + 3/2 = x(1 + \delta)$ . Since the spherical Bessel function decreases rapidly as  
 287 the order becomes larger than the argument, the parameter  $\delta$  is assumed to  
 288 be much smaller than the unit. Therefore, the error can be expressed as

$$\epsilon \simeq (2\delta)^{-1/4} e^{-x(2\delta)^{3/2}/3} \quad (\text{A.6})$$

289 The second term in this equation is much smaller than the first and then  
 290 dominates the error. Thus, taking the logarithm on both sides of this equa-  
 291 tion, we can estimate the truncation order in Eq. (6) as

$$N = \nu + kd + 1.8(\log \epsilon^{-1})^{2/3} (kd)^{1/3}. \quad (\text{A.7})$$

292 The term  $\log \epsilon^{-1}$  is closely related to the number of precision digits, which is  
 293 given by the nearest integer to  $(\log \epsilon^{-1} + 1.0 - \log 2)$ .

294 **References**

- 295 Anderson VC. Sound scattering from a fluid sphere. *J. Acoust. Soc. Am.*,  
296 1950;22:426–431.
- 297 Azarpeyvand M. Acoustic radiation force of a Bessel beam on a porous  
298 sphere. *J. Acoust. Soc. Am.*, 2012;131:4337–4348.
- 299 Chen X, Apfel R. Radiation force on a spherical object in an axisymmetric  
300 wave field and its application to the calibration of high-frequency trans-  
301 ducers. *J. Acoust. Soc. Am.*, 1996;99:713.
- 302 Colton D, Kress R. *Inverse Acoustic and Electromagnetic Scattering Theory*.  
303 Springer-Verlag, Berlin, Germany, 1998.
- 304 Courtney CRP, Ong CK, Drinkwater BW, Wilcox PD. Manipulation of mi-  
305 croparticles using phase-controllable ultrasonic standing waves (EL). *J.*  
306 *Acoust. Soc. Am.*, 2010;128:195–199.
- 307 Edwards PL, Jarzynski J. Scattering of focused ultrasound by spherical mi-  
308 croparticles. *J. Acoust. Soc. Am.*, 1983;74:1006–1012.
- 309 Embleton TFW. Mean force on a sphere in a spherical sound field. I. (The-  
310 oretical). *J. Acoust. Soc. Am.*, 1954;26:40–45.
- 311 Gor'kov LP. On the forces acting on a small particle in an acoustic field in  
312 an ideal fluid. *Sov. Phys. Dokl.*, 1962;6:773–775.
- 313 Gouesbet G, Lock JA, Grehan G. Partial-wave representations of laser beams  
314 for use in light-scattering calculations. *Appl. Opt.*, 1995;34:2133–2143.

- 315 Hasegawa T, Saka K, Inoue N, Matsuzawa K. Acoustic radiation force ex-  
316 perience by a solid cylinder in a plane progressive sound field. *J. Acoust.*  
317 *Soc. Am.*, 1988;83:1770–1775.
- 318 Hasegawa T, Yosioka K. Acoustic-radiation force on a solid elastic sphere. *J.*  
319 *Acoust. Soc. Am.*, 1969;46:1139–1143.
- 320 Kang ST, Yeh CK. Potential-well model in acoustic tweezers. *IEEE Trans.*  
321 *Ultrason. Ferroelec. Freq. Contr.*, 2010;57:1451–1459.
- 322 King LV. On the acoustic radiation pressure on spheres. *Proc. R. Soc. A*,  
323 1934;147861:212–240.
- 324 Lee J, Ha K, Shung K. A theoretical study of the feasibility of acoustical  
325 tweezers: Ray acoustics approach. *J. Acoust. Soc. Am.*, 2005;117:3273–  
326 3280.
- 327 Lee J, Shung KK. Radiation forces exerted on arbitrarily located sphere by  
328 acoustic tweezer. *J. Acoust. Soc. Amer*, 2006;120:1084–1094.
- 329 Lee J, Teh S, Lee A, Kim H, Lee C, Shung K. Single beam acoustic trapping.  
330 *Appl. Phys. Lett.*, 2009;95:073701.
- 331 Lucas BG, Muir TG. The field of a focusing source. *J. Acoust. Soc. Am.*,  
332 1982;72:1289–1289.
- 333 Marston PL. Axial radiation force of a Bessel beam on a sphere and direction  
334 reversal of the force. *J. Acoust. Soc. Am.*, 2006;120:3518–3524.
- 335 Martin PA. Multiple Scattering Interaction of Time-Harmonic Waves with  
336 *N* Obstacles. Cambridge University Press, Cambridge, UK, 2006.

- 337 Mitri FG. Negative axial radiation force on a fluid and elastic spheres illu-  
338 minated by a high-order Bessel beam of progressive waves. *J. Phys. A*,  
339 2009;42:245202.
- 340 Mitri FG, Silva GT. Off-axial acoustic scattering of a high-order Bessel vortex  
341 beam by a rigid sphere. *Wave Motion*, 2011;48:392–400.
- 342 Nyborg WL. Radiation pressure on a small rigid sphere. *J. Acoust. Soc. Am.*,  
343 1967;42:947–952.
- 344 Pierce AD. *Acoustics: An Introduction to Its Physical Principles and Appli-*  
345 *cations*. Acoustical Society of America, 1989.
- 346 Rayleigh L. On the pressure of vibrations. *Philos. Mag.*, 1902;3:338–346.
- 347 Shi J, Ahmed D, Mao X, Lin S, Lawit A, Huang T. Acoustic tweezers:  
348 patterning cells and microparticles using standing surface acoustic waves  
349 (SSAW). *Lab on a Chip*, 2009;920:2890–2895.
- 350 Silva GT. An expression for the radiation force exerted by an acoustic beam  
351 with arbitrary wavefront. *J. Acoust. Soc. Am.*, 2011a;130:3541–3545.
- 352 Silva GT. Off-axis scattering of an ultrasound Bessel beam by a sphere. *IEEE*  
353 *Trans. Ultrason. Ferroelec. Freq. Contr.*, 2011b;58:298–304.
- 354 Silva GT, Lobo TP, Mitri FG. Radiation torque produced by an arbitrary  
355 acoustic wave. *Europhys. Phys. Lett.*, 2012a;97:54003.
- 356 Silva GT, Lopes JH, Lobo TP, Mitri FG. Off-axial acoustic radiation force of  
357 pressor and tractor Bessel beams on a sphere. *IEEE Trans. Ultras. Ferroel.*  
358 *Freq. Control*, 2012b. Submitted for publication.

- 359 Song J, Chew WC. Error analysis for the truncation of multipole expansion of  
360 vector Green's functions. *IEEE Micro. Wireless Comp. Lett.*, 2001;11:311–  
361 313.
- 362 Westervelt PJ. Acoustic radiation pressure. *J. Acoust. Soc. Am.*, 1957;29:26–  
363 29.
- 364 Williams EG. *Fourier Acoustics: Sound Radiation and Nearfield Acoustical*  
365 *Holography*. Academic Press, Inc., San Diego, CA, 1999.
- 366 Wu J. Acoustical tweezers. *J. Acoust. Soc. Amer*, 1991;89:2140–2143.
- 367 Yosioka K, Kawasima Y. Acoustic radiation pressure on a compressible  
368 sphere. *Acustica*, 1955;5:167–173.

369 **Figure Captions**

370 **Figure 1:** Sketch of the acoustic scattering by a sphere placed anywhere in  
371 the host medium. The systems  $O$  and  $O'$  correspond to the on-focus  
372 and off-focus scattering configurations.

373 **Figure 2:** Pressure amplitude generated by the spherically focused trans-  
374 ducer with aperture 44 mm and F-number of 1.6, operating at 3.1 MHz.  
375 along the  $x$ -axis in the focal plane. The pressure is evaluated along (a)  
376 the transverse and (b) the axial directions.

377 **Figure 3:** Axial radiation force versus the droplet's position along  $z$  direc-  
378 tion in the focal plane. The force is computed through the PWE and  
379 Gor'kov's methods. The size factors of the sphere are (a)  $ka = 0.1$  and  
380 (b)  $ka = 0.5$ .

381 **Figure 4:** Transverse radiation force versus the droplet's position along  $x$   
382 direction in the focal plane. The force is computed through the PWE  
383 and Gor'kov's methods. The size factors are (a)  $ka = 0.1$  and (b)  
384  $ka = 0.5$ .

385 **Figure 5:** Axial radiation force versus the droplet's position along  $z$  direc-  
386 tion for the resonant scattering regime (a)  $ka = 1$  and (b)  $ka = 5$ .

387 **Figure 6:** Transverse radiation force on a silicone oil droplet (with and with-  
388 out attenuation) in the resonant scattering regime (a)  $ka = 1$  and (b)  
389  $ka = 5$ .

390 **Figure 7:** Transverse radiation force vector field in the transducer focal

391 plane produced on the silicone oil droplet in the resonant regime  $ka = 1$ .

392 The vector field is plot on top of the axial radiation force.